Measurements and Model for the Satellite-to-Aircraft Channel in L-Band

Thomas Jost[1], Wei Wang[1], Martin Schwinzerl[2],
Fernando Pérez-Fontán[3], Michael Schönhuber[2], Nicolas Floury[4]

[1]German Aerospace Center (DLR), Wessling, Germany
[2]Joanneum Research (JR), Graz, Austria
[3]Signal Theory and Communications, University of Vigo, Vigo, Spain
[4]European Space Research and Technology Centre (ESTEC), Nordwijk, The Netherlands

***Abstract*—Wireless radio transmission from a satellite based emitter to a receiver located on a aircraft is of interest for many applications such as passenger's internet access, air traffic management or positioning by global navigation satellite systems (GNSSs). Especially, the last two applications listed are related to safety-of-life functionality that requires accurate channel models for software based system testing. State-of-the art channel models for the satellite-to-aircraft case lack of accuracy in terms of modeling all propagation impairments. In this contribution, we describe the airborne experiments using Global Positioning System (GPS) signals and the data evaluation. A preliminary channel model is presented.**

I. Introduction

Electromagnetic waves transmitted from a satellite based emitter to an airborne receiver are of immense importance for communications and navigation. Applications within this scope, range from internet service to passengers while flying over remote areas up to safety-of-life related functionality like data communications for aircraft traffic management (ATM) or aircraft positioning by global navigation satellite systems (GNSSs) in different phases of flight. Radio transmission links related to safety-of-life have to be of high availability and continuity-of-service, i.e. require robust transmission links in all phases and conditions of flight. To fulfill the requirements for such stringent applications, receivers need to be adapted to the wireless propagation conditions.

The wireless radio channel for electromagnetic waves from a satellite based transmitter to an airborne located receiver is affected by several propagation impairments [1]–[3]. Atmospheric effects, ground-based originated multipath and local effects of the aircraft structure interact coherently, causing fading of the received signal amplitude. Several channel models like [1], [4], [5] able to simulate the satellite-to-aircraft propagation channel can be found in literature. These channel models can be used to develop and advance the physical layer receiver signal processing algorithms. Nevertheless, current state-of-the art channel models do not take all propagation effects accurately into account and, therefore, limiting their usability to test receiver algorithms for demanding applications. Channel models such as [1], [4] do not model the aircraft structure exhaustively such that signal blockage by the tail fin for example cannot be simulated.

Fig. 1. Overview of the four aircraft, starting at the upper left corner and moving clockwise: Aérospatiale Alouette III, Sikorsky S-70 Black Hawk, Lockheed C130 Hercules, and Pilatus Porter PC-6.

To surmount the restrictions of state-of-the art aeronautical channel models [1], [4], [5] different types of measurement campaigns were conducted within the European Space Agency (ESA) funded project "Aeronautical Satellite Communications Channel Characteristics". The effects of the aircraft structure on the receiving antenna pattern are measured by measurements on ground described in [6]. Ground reflectivity measurements for low elevation angles have been conducted above certain surface types in L- and K-band as described in [7]. At last, airborne measurements with four different aircraft shown in Fig. 1 using Global Positioning System (GPS) signals as signals of oportunity for channel sounding have been performed as described in [8]. The measurements using GPS signals are not only dedicated to measure the ground surface reflection but also to provide a full channel characterization. Within this contribution we will focus on the measurements performed using GPS signals and provide a first draft of the final channel model.

The rest of the paper is organized as follows: Section II, reviews the measurement hardware followed by a description of a flight performed using the Pilatus Porter PC-6. Section III provides the description of the performed data evaluation.

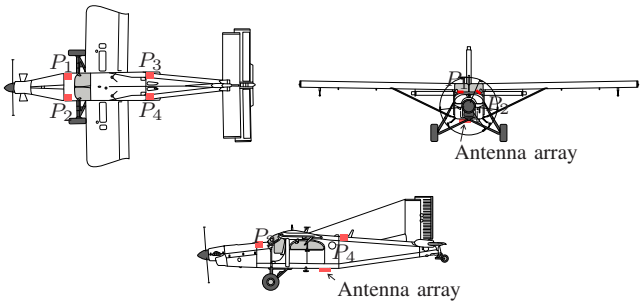

Fig. 2. Visualization of the L-band antenna positions P_1, P_2, P_3 and P_4 for the upward directed antennas for the Pilatus Porter PC-6. An additional 2x2 antenna array is mounted at the bottom of the plane.

Thereafter, Section IV provides a description of the preliminary channel model while Section V concludes the paper and gives an outlook to future works.

II. Airborne Measurements

The principle of the airborne measurements and related hardware are already described in [8], [9]. Nevertheless for the convenience of the reader, we will shortly describe the hardware setup and the flight measurements in this section that is followed by the data evaluation in the next section.

During the airborne experiments with the Pilatus Porter PC-6, eight different antennas were used. The four upward directed antennas were dual-polarized, i.e. right hand circular polarized (RHCP) and left hand circular polarized (LHCP) hemispherical GPS patch antennas. Fig. 2 visualizes the antenna positions on the Pilatus Porter PC-6 where the upward directed antennas are located at positions P_1, P_2, P_3 and P_4. The downward directed 2x2 antenna array manufactured by the German Aerospace Center (DLR) [10] consists of four individual circulary dual-polarized hemispherical patch antennas arranged on a rectangular grid. By using the antenna array located at the bottom of the aircraft, the ground originated multipath signals can be received. The measurement equipment, i.e. the datagrabber, is based on standard National Instruments (NI) equipment consisting of a sixteen channel analog-to-digital converter (ADC) and a storage module to record the sampled received signal at intermediate frequency (IF) for all eight circular dual polarized antennas. In order to sample the received signal at IF, synchronized parallel hardware lines consisting of low-noise amplifiers, filters and a de-modulator stages were build. A photographic view on the measurement equipment is given in Fig. 3.

Flight measurements with the downward directed 2x2 antenna array have been performed with the Pilatus Porter PC-6 visualized in Fig. 1. In the following, we will use flight data obtained with the Pilatus Porter PC-6 on the 28th of April 2015 in the vicinity of Vienna in Austria. The start and end point of the flight was the Brumowski Air Base of the Austrian Air Force located 5 km northwest of Tulln located close to Vienna. Fig. 4 provides an overview of the flight route using GoogleEarth™. During the flight of approximately 100 minutes different types of ground surfaces were overflown

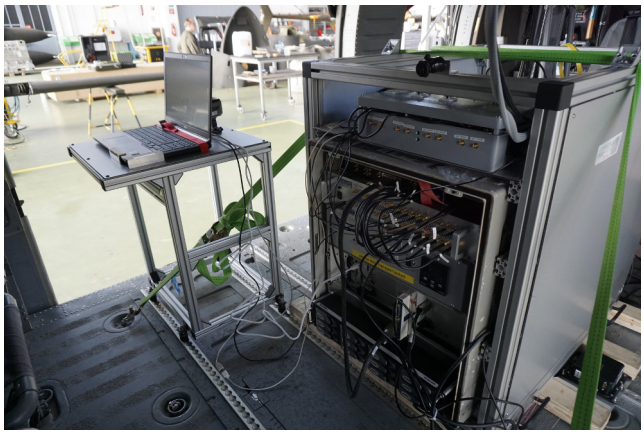

Fig. 3. Photo of the measurement equipment. In this picture, the measurement equipment was mounted inside a Sikorsky S-70 Black Hawk.

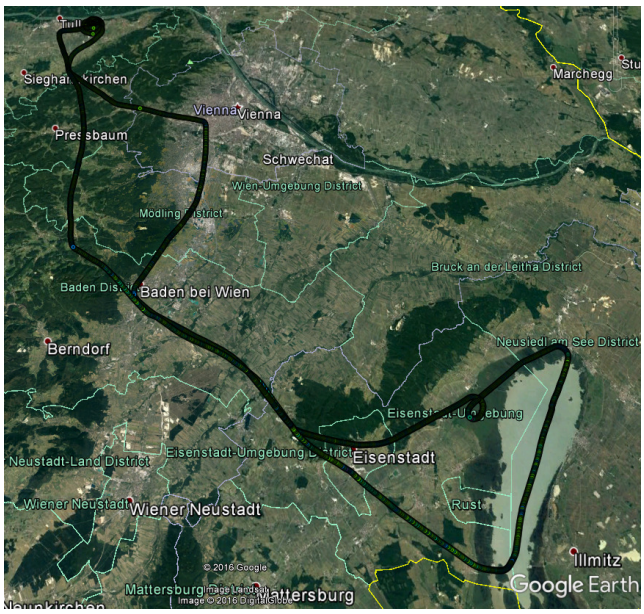

Fig. 4. Overview of the flight route flown on the 28th of April 2015. The flight started and ended at Brumowski Air Base on the upper left corner of the picture.

like large forest areas, urban areas and a water surface, i.e. lake "Neusiedler See".

III. Data Evaluation

In the post-processing, first the code phase and the Doppler are estimated for each visible satellite using the recorded signal of the upward directed antennas. Based upon complex amplitude estimation, bit changes are detected. The first processing for the upward directed antennas is based on open loop correlators, i.e. a maximum likelihood (ML) estimator with a single path assumption based on 1 ms data snapshots. In the second step, the obtained estimates are smoothed over antennas and time intervals of 500 ms to serve as initial values for the third step, i.e. the estimation of the code phase and the Doppler of the received signals at the downward

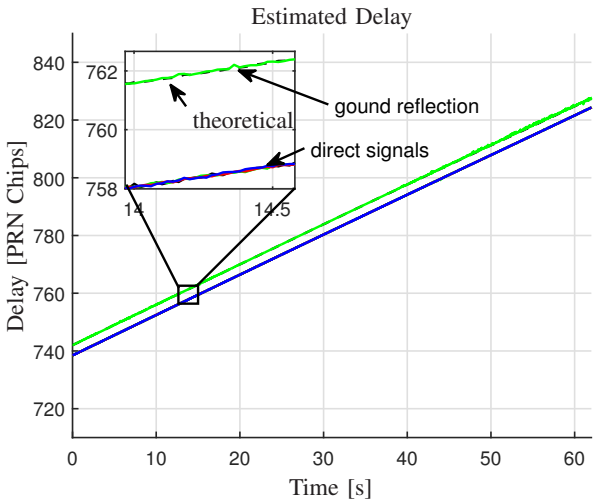

Fig. 5. Visualization of the delay estimates for different antennas. While the four upward directed antennas show a very similar delay estimate denoted as "direct signal", the estimated delay of the downward directed signal displayed as green line has an offset that fits well to the theoretical calculation displayed as dashed black curve. The data corresponds to the denoted satellite PRN 7 in Fig. 7.

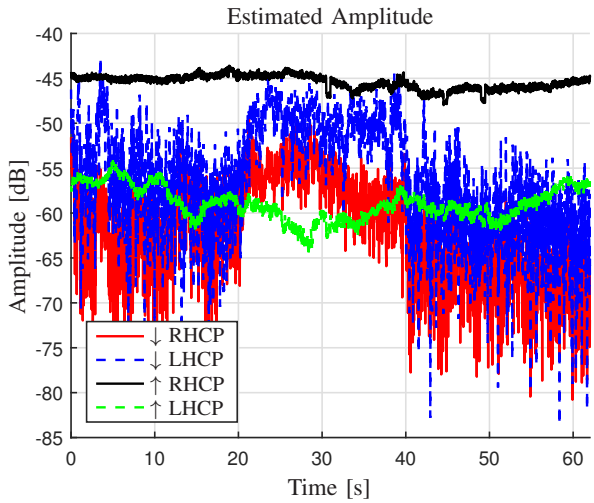

Fig. 6. Averaged estimated amplitudes for the upward (↑) and the downward (↓) directed antennas.The data corresponds to the denoted satellite PRN 7 in Fig. 7.

directed antennas. To provide a good initial value for the optimization routine of the ML estimation, the smoothed code phase result from the upward directed antennas is added to the theoretical calculation of the additional delay resulting from a ground reflection based upon the height of the aircraft above ground using Shuttle Radar Topography Mission (SRTM) and position data. To increase the post-correlator signal-to-noise ratio, 20 ms of data are used coherently. Based upon a 20 ms time grid, the amplitudes of the upward oriented and the downward oriented antennas are estimated. Fig. 5 shows an example of the code phase estimates after the third processing step. It is visible that the ground reflection can be tracked using the measured data from the downward directed antennas. Using the same data, Fig. 6 provides an exemplary view on typical final amplitude estimates for the upward and downward directed antennas.

Based on the Friis transmission equation, the theoretical received power of the line-of-sight (LoS) path can be calculated as

$$P_{r,\mathrm{LoS}} = \frac{P_t\, G_{t,\mathrm{LoS}}\, G_{r,\mathrm{LoS}}\, \lambda^2}{(4\pi\, d_{\mathrm{LoS}})^2}\,, \tag{1}$$

where $P_{r,\mathrm{LoS}}$ denotes the received power, P_t the transmit power, $G_{t,\mathrm{LoS}}$ and $G_{r,\mathrm{LoS}}$ the antenna gains at the transmitter and receiver side for the LoS path, respectively. The wavelength is denoted by λ while d_{LoS} stands for the distance between the transmit and receive antenna. The received signal power via the reflected path on ground $P_{r,\mathrm{refl}}$ can be approximated using [11]

$$P_{r,\mathrm{refl}} = \frac{P_t\, G_{t,\mathrm{refl}}\, G_{r,\mathrm{refl}}\, \lambda^2}{(4\pi\, d_{\mathrm{refl}})^2}\, |\Gamma|^2\,, \tag{2}$$

where $|\Gamma|$ stands for the absolute value of the Fresnel reflection coefficient, d_{refl} for the geometrical length of the reflected path, $G_{t,\mathrm{refl}}$ and $G_{r,\mathrm{refl}}$ for the corresponding antenna gains at the transmitter and receiver sides. Taking the ratio between (2) and (1) allows to express the absolute value of the Fresnel reflection coefficient as [11]

$$|\Gamma| = \frac{d_{\mathrm{refl}}}{d_{\mathrm{LoS}}} \sqrt{\frac{P_{r,\mathrm{refl}}\, G_{t,\mathrm{LoS}}\, G_{r,\mathrm{LoS}}}{P_{r,\mathrm{LoS}}\, G_{t,\mathrm{refl}}\, G_{r,\mathrm{refl}}}}\,. \tag{3}$$

For the airborne GPS measurements, we may assume

$$\frac{d_{\mathrm{refl}}}{d_{\mathrm{LoS}}} = \frac{d_{\mathrm{LoS}} + \Delta_{\mathrm{refl}}}{d_{\mathrm{LoS}}} \simeq 1\,, \tag{4}$$

where $d_{\mathrm{refl}} = d_{\mathrm{LoS}} + \Delta_{\mathrm{refl}}$, i.e. $d_{\mathrm{LoS}} \gg \Delta_{\mathrm{refl}}$ such that (3) can be simplified to

$$|\Gamma| \simeq \sqrt{\frac{P_{r,\mathrm{refl}}\, G_{t,\mathrm{LoS}}\, G_{r,\mathrm{LoS}}}{P_{r,\mathrm{LoS}}\, G_{t,\mathrm{refl}}\, G_{r,\mathrm{refl}}}}\,. \tag{5}$$

Assuming further that the co-polar antenna gain of the upward directed antennas for the LoS path is similar to the co-polar antenna gain of the downward directed antennas for the reflected path, i.e. $G_{r,\mathrm{refl}} \simeq G_{r,\mathrm{LoS}}$ and that the transmitter is in the far field, i.e.$G_{t,\mathrm{LoS}} \simeq G_{t,\mathrm{refl}}$, (5) simplifies to

$$|\Gamma| \simeq \sqrt{\frac{P_{r,\mathrm{refl}}}{P_{r,\mathrm{LoS}}}}\,. \tag{6}$$

Fig. 7 provides a visual representation for estimated Fresnel reflection coefficients for RHCP and LHCP signals by color while the dots represent the specular reflection points. Especially for LHCP signals, a clear distinction between water and land surface is visible.[1]

[1]At Neusiedler See a large reed area is located in before the shore. In Fig. 7, the reed area spans from roughly 16.67 ° to 16.69 ° in longitude.

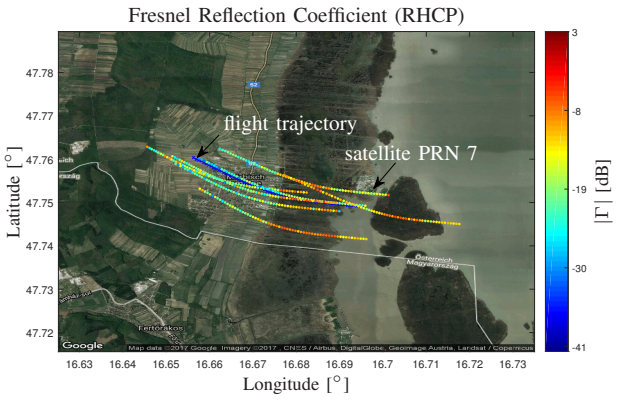

(a) Estimated Fresnel reflection coefficients for RHCP polarization.

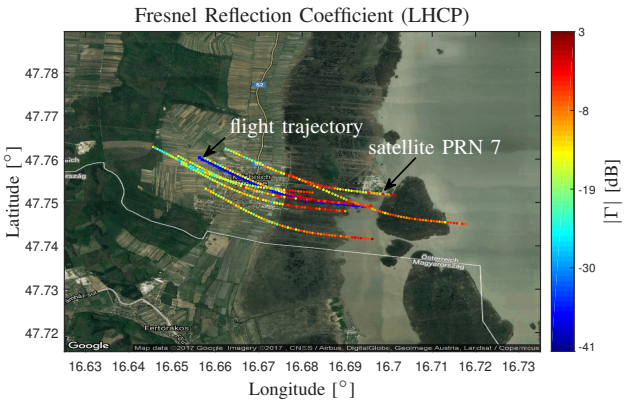

(b) Estimated Fresnel reflection coefficients for LHCP polarization.

Fig. 7. Estimated Fresnel reflection coefficients of the ground surface according to (6) for RHCP and LHCP received signals. The projected flight trajectory is displayed by blue crosses while the other trajectories represent the specular reflection points for different satellites. The absolute value of the estimated Fresnel reflection coefficient is displayed in color. The trajectory marked as satellite PRN 7 corresponds to the measurements provided in Fig. 5 and Fig. 6. Please note that the flight direction was towards in-land.

IV. Preliminary Proposed Channel Model

The structure of the preliminary proposed channel model for the satellite-to-aircraft propagation scenario is displayed in Fig. 8. The tap-delay-line structure represents the direct path and the ground reflected path. For the direct path, the complex amplitude $\alpha_{\mathrm{LoS}}(t)\, e^{-j2\pi f_c \tau_{\mathrm{LoS}}(t)}$ is calculated using the free space gain $\alpha_{\mathrm{LoS}}(t)$ and a phasor calculated using the carrier frequency f_c and the direct path propagation delay

$$\tau_{\mathrm{LoS}}(t) = \frac{\|\boldsymbol{x}_t - \boldsymbol{x}_r\|}{c}\,, \tag{7}$$

where c stands for the speed of light, $\boldsymbol{x}_t$ for the transmitter and $\boldsymbol{x}_r$ for the receiver position. The ground reflected path is additionally delayed by $\tau_{\mathrm{refl}}(t) - \tau_{\mathrm{LoS}}(t)$ where $\tau_{\mathrm{refl}}(t)$ denotes the propagation length of the reflected path divided by c. The delay $\tau_{\mathrm{refl}}(t)$ is calculated by

$$\tau_{\mathrm{refl}}(t) = \tau_{\mathrm{LoS}}(t) + \frac{2\,h(t)}{c} \sin\left(\epsilon_{\mathrm{LoS}}(t)\right)\,, \tag{8}$$

where $h(t)$ denotes the receiver position above ground and $\epsilon_{\mathrm{LoS}}(t)$ the elevation angle of the satellite seen from the receiver in horizontal position. Please note that the assumption of a planar Earth is used in (8). The amplitude of the reflected path is adjusted by the term $\Gamma(t)e^{-j2\pi f_c(\tau_{\mathrm{refl}}(t)-\tau_{\mathrm{LoS}}(t))}$ representing the additional gain through the reflection on Earth's surface. The process $\Gamma(t)$ depends generally on the type of surface. Therefore, it has been modeled as a time-variant Rician process whose parameters are derived from the measurement data described in the previous sections. Both, direct and reflected paths are affected by the antenna pattern $G(\phi, \epsilon)$ that is influenced by the airborne structure. The antenna pattern $G(\phi, \epsilon)$ in dependence of the azimuth ϕ and elevation angle ϵ affected by the airborne structure is denoted as "Modified Antenna Pattern" in Fig. 8. The modified antenna pattern needs to be calculated prior to simulations by electromagnetic tools as it highly depends on the aircraft structure, the antenna itself as well as its position on the aircraft.

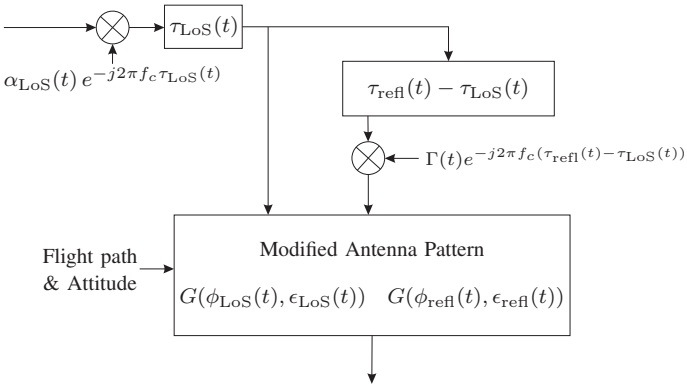

Fig. 8. Model structure of the preliminary channel model.

V. Conclusion and Outlook

State-of-the art satellite-to-aircraft channel models miss certain details on propagation effects. In order to test physical layer receiver signal processing algorithms for applications that require robust transmission links, novel propagation channel models have to be developed. To develop a new satellite-to-aircraft channel model in L-band, measurements taking GPS L1 C/A signals as signals of opportunity have been conducted. A preliminary channel model for the satellite-to-aircraft scenario is presented.

Acknowledgement

Work in this project has been conducted under ESA/ESTEC ARTES 5.1 program, contract no. 4000106833/12/NL/CLP "Aeronautical Satellite Communications Channel Characteristics" and in cooperation with the Austrian Armed Forces. The writers of this paper would also like to thank their colleagues

Balázs Matuz and Michael Walter (DLR) for their valuable contributions and support during the design and execution of the experiments.

REFERENCES

[1] P. A. Bello, "Aeronautical Channel Characterization," *IEEE Trans. Commun.*, vol. COM-21, no. 5, pp. 548–563, May 1973.

[2] A. Miura, S. Yamamoto, H.-B. Li, M. Tanaka, and H. Wakana, "Ka-Band Aeronautical Satellite Communications Experiments Using COMETS," *IEEE Trans. Veh. Technol.*, vol. 51, no. 5, pp. 1153–1164, Sep. 2002.

[3] M. Holzbock and C. Senninger, "An Aeronautical Multimedia Service Demonstration at High Frequencies," *IEEE Multimedia*, vol. 6, no. 4, pp. 20–29, Oct. 1999.

[4] A. Steingass, A. Lehner, F. Pérez-Fontán, E. Kubista, and B. Arbesser-Rastburg, "Characterization of the aeronautical satellite navigation channel through high-resolution measurement and physical optics simulation," *Int. J. Satell. Commun. Network*, vol. 26, no. 1, pp. 1–30, 2008.

[5] ITU-R, "Propagation data required for the design of Earth-space aeronautical mobile telecommunication systems," Tech. Rep. ITU-R P.682-3, 2012.

[6] M. Schwinzerl, T. Jost, F. Pérez-Fontán, M. Schönhuber, W. Wang, M. Walter, T. Pelzmann, G. Obertaxer, N. Floury, and R. Prieto-Cerdeira, "Wide-Band Characterization of Antennae Plus Aircraft Platform Patterns in L- and Ka-Band," in *EuCAP*, Apr. 2015.

[7] T. Jost, M. Schwinzerl, W. Wang, T. Pelzmann, G. Obertaxer, M. Walter, M. Schönhuber, and N. Floury, "Ground Reflection for Low Elevations at L- and K-Band," in *EuCAP*, Apr. 2016.

[8] T. Pelzmann, T. Jost, M. Schwinzerl, F. Pérez-Fontán, M. Schönhuber, and N. Floury, "Airborne measurements enhancing the satellite-to-aircraft channel model in L-band," in *EuCAP*, Apr. 2016.

[9] T. Jost, T. Pelzmann, M. Schwinzerl, M. Walter, M. Schönhuber, and N. Floury, "Using Airborne Measurements to Model the Satellite-to-Aircraft Channel Model at L-Band," in *EuCAP*, Mar. 2017.

[10] M. Heckler, M. Cuntz, A. Konovaltsev, L. Greda, A. Dreher, and M. Meurer, "Development of Robust Safety-of-Life Navigation Receivers," *IEEE Trans. Microw. Theory Tech.*, vol. 59, no. 4, pp. 998–1005, Apr. 2011.

[11] O. Landron, M. Feuerstein, and T. Rappaport, "A Comparison of Theoretical and Empirical Reflection Coefficients for Typical Exterior Wall Surfaces in a Mobile Radio Environment," *IEEE Trans. Antennas Propag.*, vol. 44, no. 3, pp. 341–351, Mar. 1996.